Research Square

Preprints are preliminary reports that have not undergone peer review.
They should not be considered conclusive, used to inform clinical practice,
or referenced by the media as validated information.

Study of the performance of ab-initio theoretical methods in electronic excited states, by predicting the structure of some aromatic molecules already reported experimentally in the gas phase

Jaime Valdez Ruvalcaba

j.valdez@ugto.mx

Universidad de Guanajuato

América Y. Torres Boy

Fritz Bauer Institut

Carlos Tadeo Aguilar Mondelo

Université de Strasbourg

José Luis Cabellos Quiroz

Universidad Politécnica de Chiapas

Leonardo Álvarez Valtierra

Universidad de Guanajuato

Research Article

Keywords:

Posted Date: November 19th, 2026

DOI: https://doi.org/10.21203/rs.3.rs-11626970/v1

License: This work is licensed under a Creative Commons Attribution 4.0 International License.
Read Full License

Additional Declarations: No competing interests reported.

Study of the performance of *ab-initio* theoretical methods in electronic excited states, by predicting the structure of some aromatic molecules already reported experimentally in the gas phase

Jaime Valdez-Ruvalcaba · América Y. Torres-Boy · Carlos T. Aguilar-Mondelo · José L. Cabellos-Quiroz · Leonardo Álvarez-Valtierra

November 4, 2026

Abstract Structural reference databases for electronically excited states (S_1) are notoriously scarce compared to ground-state reference data, making the spectral assignment of gas-phase high-resolution spectra a challenging task. To overcome this limitation, this work presents a systematic evaluation of Time-Dependent Density Functional Theory (TD-DFT) using 15 exchange-correlation functionals paired with 7 basis sets; alongside, the Configuration Interaction Singles (CIS) method is tested across the same basis sets. The predictive structural capability of all 112 theoretical combinations was evaluated on 11 mostly planar aromatic molecules by comparing calculated inertial parameters against experimental gas-phase rotational constants using a weighted Root-Mean-Square Difference (RMSD) approach. By summation of the RMSD values across all evaluated systems, the study allows us to identify the optimal

J. Valdez-Ruvalcaba
División de Ciencias e Ingenierías, Campus León, Universidad de Guanajuato, Loma del Bosque 103, Lomas del Campestre, 37150 León, Gto., México.
E-mail: j.valdez@ugto.mx

América Y. Torres-Boy
Current address: Molecular Physics Department. Fritz Haber Institute; Berlin, Germany 14195.
E-mail: a.torresby@gmail.com

Carlos T. Aguilar-Mondelo
Current address: M1 EUR CSC University of Strasbourg; Strasbourg, France 67081
E-mail: tadeo3020@gmail.com

José L. Cabellos-Quiroz
Universidad Politécnica de Tapachula. Tapachula, Chis. México 30830.
E-mail: jose.cabellos@uptapachula.edu.mx

L. Álvarez-Valtierra
División de Ciencias e Ingenierías, Campus León, Universidad de Guanajuato, Loma del Bosque 103, Lomas del Campestre, 37150 León, Gto., México.
E-mail: leoav@fisica.ugto.mx

method–basis set combination, providing a cost-effective and reliable theoretical protocol for predicting excited-state geometries.

Keywords TD-DFT · CIS · Excited Electronic States · Rotational Constants · High-Resolution Electronic Spectroscopy · RMSD Evaluation · Gas Phase

1 Introduction

For the past few decades, high-resolution experiments utilizing rotationally resolved UV spectrometers in the gas phase have demonstrated outstanding synergy with molecular ground state (S_0) quantum chemical calculations. For the computed S_0 inertial parameters; specifically, the rotational constants (A'', B'', and C'') consistently align with high accuracy alongside experimental values extracted from the high resolution electronic spectral fits. However, an accurate prediction of the inertial parameters of the first electronically excited singlet state (S_1) has historically encountered a much lower rate of success compared to the ground state configurations [1].

In the workflow of analyses of high-resolution electronic spectra, a precise fitting procedure of the experimental traces begins by providing a theoretical accurate set of rotational constants for both the ground and the excited electronic state, which constitute the "initial guess" of the inertial parameters. While high-level electronic structure calculations routinely supply the ground-state baseline, the initial parameters for the S_1 state have frequently been guessed by the user. This gap stems primarily from the notable scarcity of systematic structural reference data for electronic excited states compared to the ground state. This scarcity is a direct consequence of the inherent complexity of accurately capturing electron correlation during electronic transitions, combined with the limited availability of high-resolution gas-phase experimental data for molecular systems. Such a lack of preliminary, accurate S_1 structural theoretical models renders the fitting procedure highly challenging, since the starting S_1 inertial parameters may be significantly far away from the true experimental values.

Besides the rotational constants input for both electronic states, the absolute electronic origin frequency is also required. Guided by specific spectral selection rules derived from the orientation of the transition dipole moment vector, a simulated rotationally resolved spectrum is generated. Rotational lines are manually assigned to the experimental data, and a least-squares minimization routine optimizing the "Observed-Minus-Calculated" (OMC) line positions is executed to refine the constants iteratively. The spectrum is considered successfully fit when the global OMC deviation drops below one-tenth of the Full Width at Half Maximum (FWHM) of a single rotational transition [2]. Modern frameworks also successfully leverage automated computer-based Genetic Algorithms (GA) to assist in this convergence [3].

To overcome these structural uncertainties, this work presents a systematic statistical evaluation aimed to identify an optimal computational methodol-

ogy for predicting S_1 rotational constants. Using Gaussian 16W [4], we evaluated 112 theoretical combinations (15 TD-DFT functionals [5,6] and CIS [7] combined with 7 basis sets) on 11 organic systems: 1-hydroxynaphthalene, 2-hydroxynaphthalene [8], 1-naphthoic acid [9], 7-azaindole [10], 3-methylanisole [11], 3-toluidine [12], 2,5-diphenylfuran, 2,5-diphenyl-1,3,4-oxadiazole [13], 4-methylanisole [14], 1,3-benzodioxole [15], and 9-fluorenemethanol [16]. Through a weighted RMSD scheme, we determine the most accurate theoretical methods to guide the high-resolution electronic spectra fitting procedures.

2 Theoretical Methods

Two widely used quantum chemical frameworks: Time-Dependent Density Functional Theory (TD-DFT) and Configuration Interaction Singles (CIS) have been tested and analyzed for S_1 electronic excited states. While TD-DFT is conventionally favored for incorporating dynamic electron correlation through various exchange-correlation kernels, the *ab-initio* CIS method was considered as a fundamental, computationally efficient wavefunction-based reference that inherently operates without functional dependencies.

To ensure an unbiased and comprehensive assessment, a systematic matrix of density functionals and basis sets was constructed. For the TD-DFT calculations, we considered a selection of 15 exchange-correlation functionals designed to capture different physical treatments of molecular electronic structures. This selection encompasses local generalized gradient approximation (GGA) functionals (PBEPBE and BLYP) [17,18], a functional with dispersion correction (B97D3) [19], a meta-GGA functional (M06L), and a broad series of hybrid functionals (PBE1PBE, B3LYP, B3PW91, BMK, M05, M052X, M06, M062X, and M062HF) [20–25]. Furthermore, to adequately model long-range non-bonded interactions that are non-negligible for a balanced treatment of conjugated systems, Grimme's empirical dispersion corrections (GD3) were systematically incorporated into all DFT calculations [19].

Moreover, the basis sets chosen for this work comprise seven configurations split into two main families: six split-valence Pople-type basis sets: the 6-31G [26,27] and 6-311G [28,29] families (known for their remarkable versatility and balance between computational accuracy and cost, incorporating polarization and diffuse functions) and a high-level correlation-consistent Dunning-type basis set (AUG-cc-pVTZ) [30,31] included to evaluate the impact of explicit basis set complexity on structural prediction. Table 1 summarizes the methods and basis sets used in our calculations.

Table 1 Electronic Structure Methods and Basis Sets Considered in This Work

Method Type	**Core Method / Functional**[a]
Ab initio (Wavefunction)	CIS
TD-DFT (GGA)	PBEPBE, BLYP
TD-DFT (Hybrid GGA)	PBE1PBE, B3LYP, B3PW91, BMK
TD-DFT (Minnesota Hybrid / Meta)	M05, M052X, M06, M062X, M062HF, M06L
TD-DFT (Dispersion Corrected)	B97D3

[a] Evaluated across: 6-31G, 6-31G(d,p), 6-31+G(d,p), 6-311G, 6-311G(d,p), 6-311+G(d,p), and AUG-cc-pVTZ.

To evaluate the directional accuracy of each configuration, the signed percentage difference (δ) was calculated independently along each principal inertial axis [32] as follows:

$$\delta = \left(\frac{X_{\text{calc}} - X_{\text{exp}}}{X_{\text{exp}}} \right) \times 100 \tag{1}$$

Where X represents the corresponding rotational constant (A, B, or C). The "delta" parameter provides an explicit indicator of axes-specific deviations, highlighting systematic overestimations or underestimations of the molecular framework under the specific level of theory and numerical basis set selected.

To perform the numerical analysis, a Root Mean Square Difference (RMSD) method is used, which requires the following set of equations:

$$a = \frac{A_{\text{calc}}}{A_{\text{calc}} + B_{\text{calc}} + C_{\text{calc}}} \tag{2}$$

$$b = \frac{B_{\text{calc}}}{A_{\text{calc}} + B_{\text{calc}} + C_{\text{calc}}} \tag{3}$$

$$c = \frac{C_{\text{calc}}}{A_{\text{calc}} + B_{\text{calc}} + C_{\text{calc}}} \tag{4}$$

$$\text{RMSD} = \sqrt{a(A_{\text{exp}} - A_{\text{calc}})^2 + b(B_{\text{exp}} - B_{\text{calc}})^2 + c(C_{\text{exp}} - C_{\text{calc}})^2} \tag{5}$$

In which A_{calc} is the simulated value of the rotational constant A, A_{exp} is the experimental value of the rotational constant A, and so on. The dimensionless value acquired by equations (2), (3), and (4) is used to give a certain weight to the rotational constants while using the RMSD equation (5).

Next, the RMSD is computed using the set of equations described above, and this process is repeated for each one of the method/numerical basis set combination on every molecule under study. Finally, the cumulative RMSD

value for each method/basis set is computed, adding the values over each molecule under analysis, namely:

$$\text{Cumulative RMSD} = \sum_{i=1}^{11} \text{RMSD}_i \tag{6}$$

The sum in equation 6 was made for each of the 112 method-basis set combinations, and the combination with the lowest comulative RMSD is considered "the most accurate method".

3 Results and Discussion

Tables 2 through 6 display the differences between calculated and experimental S_1 rotational constants (Δ = Calc − Exp) for a curated subset of 19 representative theoretical combinations alongside experimental values. This subset was systematically selected to cover all major functional families (GGA, hybrid GGA, Minnesota meta-GGA, and dispersion-corrected DFT), the reference *ab-initio* CIS method, and the progression of basis set expansion from double-ζ (6-31G) up to augmented triple-ζ (aug-cc-pVTZ) quality, including top-performing models such as M06-2X. The complete set of tables for the remaining 6 molecules studied is available in the Supplementary Information.

1,3-Benzodioxole

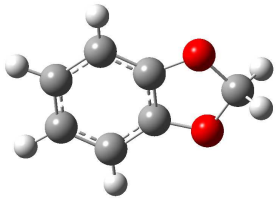


Table 2 Differences between calculated and experimental S_1 rotational constants (Δ = Calc − Exp, in MHz) for 1,3-Benzodioxole. Experimental values: $A' = 3628.8$, $B' = 1628.4$, $C' = 1136.4$ MHz.

Computational Method	$\Delta A'$ **(MHz)**	$\Delta B'$ **(MHz)**	$\Delta C'$ **(MHz)**
PBE1PBE/6-31G(d)	-0.7	-38.1	-22.7
PBE1PBE/6-311G	+10.9	-34.2	-19.7
PBEPBE/6-31G	-65.1	-72.2	-45.3
B97D3/6-31G	-69.9	-78.1	-48.7
B3LYP/6-311G	-14.8	-53.5	-31.6
BLYP/6-31G	-91.2	-89.4	-56.2
BP86/6-31G	-78.4	-77.1	-49.0
BPBE/6-31G	-71.8	-73.6	-46.7
B3PW91/6-31G	-12.7	-45.4	-27.4
BMK/6-31G	-33.4	-46.4	-29.8
M05/6-31G	+1.9	-41.0	-23.9
M052X/6-31G	+1.0	-36.2	-21.6
M052X/6-31G(d,p)	+30.9	+6.6	+2.0
M06L/6-31G	-10.2	-50.4	-29.7
M06/6-31G	+7.6	-37.1	-21.4
M062X/6-311G	+5.8	-35.8	-20.9
M062X/6-311G(d,p)	+40.2	+9.4	+4.3
M062X/6-311++G(d,p)	+40.2	+12.9	+6.0
M062X/aug-cc-pVTZ	+54.6	+19.4	+10.5
M06HF/6-31G	+12.0	-36.4	-20.6
CIS/6-31G	+86.9	-28.4	-10.0
CIS/6-311G(d,p)	+114.0	+20.6	+16.7
CIS/aug-cc-pVTZ	+177.4	+65.6	+44.8

2,5-Diphenylfuran

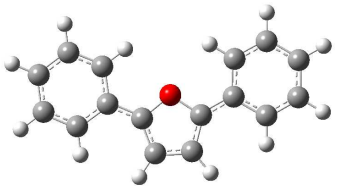


Table 3 Differences between calculated and experimental S_1 rotational constants (Δ = Calc − Exp, in MHz) for 2,5-Diphenylfuran. Experimental values: $A' = 1456.5$, $B' = 218.8$, $C' = 190.0$ MHz.

Computational Method	$\Delta A'$ **(MHz)**	$\Delta B'$ **(MHz)**	$\Delta C'$ **(MHz)**
PBE1PBE/6-31G(d)	-24.4	-2.4	-2.0
PBEPBE/6-31G	-49.0	-5.9	-5.0
B97D3/6-31G	-40.8	-7.2	-5.9
B3LYP/6-311G	-25.1	-4.2	-3.4
BLYP/6-31G	-50.0	-8.3	-6.9
B3PW91/6-31G	-27.1	-3.4	-2.8
M052X/6-31G	-17.2	-2.0	-1.6
M052X/6-31G(d,p)	-17.6	+0.8	+0.5
M06/6-31G	-31.7	-1.2	-1.2
M062X/6-311G	-14.1	-2.4	-1.8
M062X/6-311G(d,p)	-10.2	+0.5	+0.4
M062X/aug-cc-pVTZ	+2.5	+0.9	+1.0
M06HF/6-31G	-23.3	-1.2	-1.1
CIS/6-31G	-1.4	-1.4	-0.9
CIS/6-311G	+0.1	-1.1	-0.6
CIS/6-31G(d,p)	+2.8	+0.9	+0.9
CIS/6-311G(d,p)	+5.5	+1.1	+1.2
CIS/6-311+G(d,p)	-1.7	+1.2	+1.1
CIS/aug-cc-pVTZ	+15.4	+1.9	+1.9

7-Azaindole

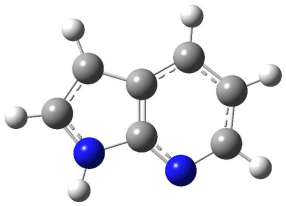


Table 4 Differences between calculated and experimental S_1 rotational constants (Δ = Calc − Exp, in MHz) for 7-Azaindole. Experimental values: $A' = 3744.4$, $B' = 1701.7$, $C' = 1170.5$ MHz.

Computational Method	$\Delta A'$ **(MHz)**	$\Delta B'$ **(MHz)**	$\Delta C'$ **(MHz)**
PBE1PBE/6-31G(d)	+134.2	-42.9	-8.6
PBEPBE/6-31G	+65.2	-76.6	-31.4
B97D3/6-31G	+64.8	-81.3	-33.7
B3LYP/6-311G	+124.3	-57.0	-16.4
BLYP/6-31G	+43.8	-90.9	-40.3
BP86/6-31G	+53.2	-81.3	-34.7
B3PW91/6-31G	+122.6	-49.6	-13.0
BMK/6-31G	+99.8	-52.8	-16.6
M05/6-31G	+126.3	-45.4	-10.5
M052X/6-31G	+147.0	-37.2	-4.7
M052X/6-31G(d,p)	+152.4	-13.0	+7.7
M06/6-31G	+130.0	-42.8	-9.0
M062X/6-311G	+145.7	-40.6	-6.5
M062X/6-311G(d,p)	+160.5	-14.9	+7.5
M062X/aug-cc-pVTZ	+177.8	-7.9	+12.4
M06HF/6-31G	+363.4	-100.8	-18.0
CIS/6-31G	+170.4	-16.9	+7.4
CIS/6-311G(d,p)	+170.8	+10.2	+20.6
CIS/aug-cc-pVTZ	+194.1	+19.4	+27.2

3-Methylanisole

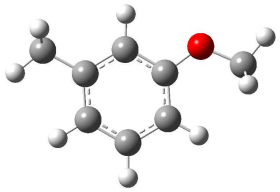


Table 5 Differences between calculated and experimental S_1 rotational constants (Δ = Calc − Exp, in MHz) for 3-Methylanisole. Experimental values: $A' = 3406.5$, $B' = 1111.3$, $C' = 847.2$ MHz.

Computational Method	$\Delta A'$ **(MHz)**	$\Delta B'$ **(MHz)**	$\Delta C'$ **(MHz)**
PBE1PBE/6-31G(d)	+8.0	-10.5	-6.0
PBEPBE/6-31G	-43.3	-13.3	-21.3
B97D3/6-31G	-52.8	-35.2	-24.0
B3LYP/6-311G	-13.2	-20.5	-13.1
BLYP/6-31G	-72.2	-43.4	-29.9
BP86/6-31G	-56.3	-34.8	-23.9
B3PW91/6-31G	-5.6	-15.3	-9.6
BMK/6-31G	-36.4	-18.7	-13.4
M05/6-31G	-7.6	-14.6	-9.3
M052X/6-31G	+19.2	-8.5	-4.2
M052X/6-31G(d,p)	+36.8	+9.6	+7.5
M06/6-31G	+8.7	-8.2	-4.5
M062X/6-311G	+9.5	-8.4	-4.7
M062X/6-311G(d,p)	+31.0	+11.1	+8.0
M062X/aug-cc-pVTZ	+51.5	+15.9	+12.0
M06HF/6-31G	+15.2	-10.0	-5.2
CIS/6-31G	+43.9	-7.7	-2.3
CIS/6-311G(d,p)	+61.8	+12.9	+10.8
CIS/aug-cc-pVTZ	+110.0	+24.0	+21.2

2,5-Diphenyl-1,3,4-oxadiazole

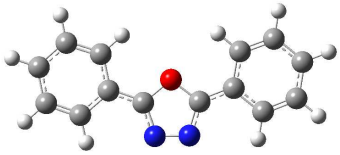


Table 6 Differences between calculated and experimental S_1 rotational constants (Δ = Calc − Exp, in MHz) for 2,5-Diphenyl-1,3,4-oxadiazole. Experimental values: $A' = 1629.9$, $B' = 213.5$, $C' = 188.5$ MHz.

Computational Method	$\Delta A'$ **(MHz)**	$\Delta B'$ **(MHz)**	$\Delta C'$ **(MHz)**
PBE1PBE/6-31G(d)	+1.2	-3.7	-2.6
PBEPBE/6-31G	-2.0	-10.4	-7.9
B97D3/6-31G	+4.0	-11.3	-8.5
B3LYP/6-311G	-12.9	-4.9	-3.7
B3LYP/6-311G(d,p)	-0.5	-1.3	-0.8
BLYP/6-31G	-7.3	-12.4	-9.6
B3PW91/6-31G	-6.6	-4.4	-3.3
M052X/6-31G	+8.0	-3.0	-2.0
M052X/6-31G(d,p)	+16.5	+0.0	+0.5
M06/6-31G	+0.9	-3.3	-2.3
M062X/6-311G	+10.6	-3.5	-2.3
M062X/6-311G(d,p)	+25.9	-0.3	+0.4
M062X/aug-cc-pVTZ	+16.9	+1.2	+1.4
CIS/6-31G	+32.9	-2.3	-1.1
CIS/6-311G(d,p)	+44.5	+1.0	+1.6
CIS/aug-cc-pVTZ	+46.1	+2.0	+2.4

3.1 Performance Analysis Across Functionals and System Types

Across the test set, hybrid functional families particularly Minnesota hybrids (M062X, M05, M052X) and BMK consistently show the best agreement with experimental S_1 rotational constants. M062X/6-311G achieves high accuracy for rigid structures like 1,3-benzodioxole (Table 2), yielding $\Delta A' = +5.8$, $\Delta B' = -35.8$, and $\Delta C' = -20.9$ MHz compared to experimental values ($A' = 3628.8$, $B' = 1628.4$, $C' = 1136.4$ MHz).

In contrast, CIS calculations systematically overestimate rotational constants due to the absence of dynamic correlation, which leads to over-contracted excited-state geometries. For example, in 1,3-benzodioxole [10], CIS/aug-cc-pVTZ overpredicts A' by +177.4 MHz (3806.2 MHz vs. 3628.8 MHz exp.).

Specific systems pose higher challenges: 7-azaindole [10] (Table 4) exhibits larger deviations due to anomalous effects driven by the single nitrogen substitution for the C7 carbon atom. Following the insights of Kim and Bernstein, these deviations arise from strong π–$n\pi^*$ state mixing and the out-of-plane displacement of the pyrrole N-H hydrogen atom in the S_1 state, leading to unique changes in its electronic distribution. Also 4-methylanisole exhibits increased errors due to low barrier methyl internal rotation effects that shift effective experimental constants away from static equilibrium structures.

3.2 Signed Relative Error Distribution (δ) for M062X/6-311G

Figure 1 illustrates the distribution of signed percentage differences (δ) across all 11 molecules calculated at the M062X/6-311G level. The rotational constants B' (orange) and C' (yellow) show tight, unimodal distributions shifted slightly into the negative side ($0 > \delta \geq -2.0\%$), indicating a minor, predictable overexpansion of computed geometries along transverse axes. Peak densities occur at $\delta = -0.5\%$ for B' and $\delta = -1.0\%$ for C'.

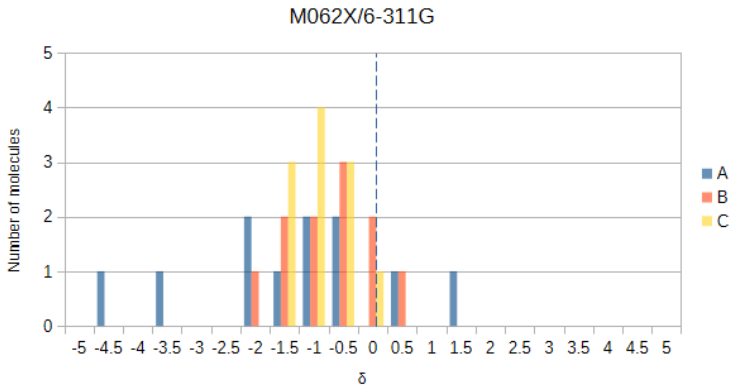


Fig. 1 Distribution of percentage difference (δ) along the principal axes (A', B', C') for the 11 studied molecules using M062X/6-311G. Vertical dashed line indicates zero error.

The A' rotational constant (blue) shows a wider spread, with most values between $\delta = +1.5\%$ and -2.0%, but with two noticeable negative outliers ($\delta = -3.5\%$ and -4.5%). These outliers reflect challenging systems like 7-azaindole, where single-reference TD-DFT faces difficulty capturing strong local charge transfer interactions.

3.3 Method Ranking via Cumulative RMSD

To determine the overall top-performing methodology, the individual RMSD values for each molecule (Equations 2–5) were summed across all 11 studied systems to calculate the Cumulative RMSD for each of the 112 theoretical combinations (Equation 6). Table 7 lists the top 12 method/basis set combinations ranked by cumulative RMSD.

Table 7 Top 12 theoretical combinations ranked by Cumulative RMSD across all 11 studied molecules.

Rank	Functional / Basis Set	Cumulative RMSD
1	**M062X / 6-311G**	**322.28**
2	M062X / 6-31G	326.63
3	BMK / 6-311G	329.08
4	BMK / 6-311+G	332.63
5	M05 / 6-31G	334.17
6	M05 / 6-311G	334.93
7	B3PW91 / 6-311G	339.00
8	B3LYP / 6-31G	344.11
9	PBE1PBE / 6-31G	345.52
10	BMK / 6-31G	345.93
11	M06L / 6-311G	346.31
12	M052X / 6-31G	347.84

M062X/6-311G achieves the lowest cumulative RMSD value of **322.28**, ranking first overall. Functionals with high Hartree-Fock exchange fractions (e.g., M062X with 54% HF exchange) perform better because reduced self-interaction error improves the description of excited-state electron density distribution. The triple-ζ 6-311G basis provides adequate radial flexibility without over-softening the potential energy surface, establishing M062X/6-311G as an optimal, computationally efficient level of theory for predicting the excited-state rotational constants.

4 Conclusions

This statistical evaluation of 112 theoretical combinations on 11 aromatic molecules establishes a quantitative comparison for predicting S_1 electronic excited-state rotational constants. Based on cumulative weighted RMSD analysis against experimental data, M062X/6-311G provides the overall best predictive accuracy with a cumulative RMSD of 322.28.

High-exchange hybrid functionals like M062X effectively mitigate self-interaction errors in $\pi \rightarrow \pi^*$ transitions, while the 6-311G basis offers sufficient flexibility without diffuse function-induced potential softening. CIS systematically overcontracts S_1 structures due to lack of dynamic correlation, making occasional close matches (e.g., 2,5-diphenylfuran) a result of error cancellation [10].

Overall, TD-DFT yields reliable longitudinal geometries (a axis) accompanied by a minor, predictable overexpansion ($0 > \delta \geq -2.0\%$) along transverse axes (b and c). M062X/6-311G is recommended as a robust standard initial guess protocol for high-resolution spectroscopic fittings.

5 Supplementary

5.1 Experimental background

The experimental excited-state inertial parameters for the molecules studied in this work were obtained from an ultra-high resolution UV spectrometer in the gas phase. Such a spectrometer consists of (1) a light generation laboratory, (2) a molecular beam machine apparatus, and (3) the signal acquisition system.

In terms of the light generation laboratory (1), it is constituted by a holographic floating optical table, where a 514.5 nm Spectra-Physics 171 Ar+ laser pumps a modified Spectra Physics 380 ring dye laser with an intracavity frequency doubling (either BBO or KDP) crystal. The SP-380 laser works with a broadband width of about 1 MHz in the fundamental, owing to all the optical components inside the cavity and its extra-cavity reference station. Depending on the dye used (Rhodamines, Kyton red, or DCM), the monochromatic fundamental light obtained may vary from about 560 nm up to about 680 nm. The fundamental light is both absolutely and relatively calibrated, using an iodine gas cell and an in-house built Fabry-Perot interferometer. Therefore, the intracavity-generated UV light may be in the range from about 280 nm to about 340 nm, depending on the dye used. The UV light is directed and focused to a differentially pumped beam machine, which perpendicularly excites the gas phase molecules.

The beam machine (2) consists of two stainless steel chambers connected by a 1 cm diameter beam skimmer. Each of the chambers has a diffusion pump attached, and both are connected to a mechanical vacuum line. Each chemical sample is added to a quartz nozzle, which is heated up to vaporize the sample and carried by an argon flow (of about -15 psi) through it. At the nozzle tip, the Joule-Thompson phenomenon takes place, and the gas sample gets its temperature dropped to about 4 or 5 Kelvin. The gas molecules do not condense since they supersonically travel in one direction in a collision-free environment. About 10 cm downstream of the nozzle tip, the molecular beam gets skimmed, and about 15 cm further, it gets perpendicularly crossed by the UV light (coming from the laser system).

By a set of collecting optics, the Fluorescence signal is detected (3) by a Hamamatsu Photo-Multiplier Tube (PMT), and the signal is discriminated, counted, and sent to a computer. The computer simultaneously collects the PMT signal, the Iodine cell signal, and the Fabry Perot (markers) signal, so that the PMT signal might be later calibrated [33]. For the molecular spectral analyses, the Windows-based Jet/beam 95 (jb95) program was used [34], where estimates of inertial parameters are introduced to the program as a starting

point; then, a simulated spectrum is obtained. Later, by assigning rotational lines from the simulated spectrum to the corresponding positions of the experimental one, the inertial parameters get optimized by running a least squares routine. By gradually increasing the number of corrected assigned lines, the simulated spectrum gets closer and closer to the experimental one, until the difference of the observed minus calculated (OMC) of the overall assigned line is less than 1/10 of the full width at half maximum (FWHM) of a single line in the spectrum. At this stage, it is considered that the experimental spectrum is fit, and the simulated inertial parameters do correspond to the experimental trace under analysis.

The molecular systems under study in this paper had previously been studied experimentally; so, the experimental ground and the first electronically excited state inertial parameters are already known.

5.2 Additional Tables

Table 8 Differences between calculated and experimental S_1 rotational constants (Δ = Calc − Exp, in MHz) for 1-Hydroxynaphthalene. Experimental values: $A' = 1923.9$, $B' = 1105.8$, $C' = 702.5$ MHz.

Computational Method	$\Delta A'$ **(MHz)**	$\Delta B'$ **(MHz)**	$\Delta C'$ **(MHz)**
PBE1PBE/6-31G(d)	+40.0	-6.2	+2.4
PBEPBE/6-31G	+12.2	-23.2	-8.2
B97D3/6-31G	+6.6	-25.7	-9.9
B3LYP/6-311G	+30.1	-11.6	-1.1
BLYP/6-31G	-2.4	-30.6	-13.1
BP86/6-31G	+6.2	-25.9	-10.0
B3PW91/6-31G	+34.5	-9.6	+0.3
BMK/6-31G	+20.8	-17.5	-4.7
M05/6-31G	+34.1	-8.2	+0.8
M052X/6-31G	+43.9	-2.8	+4.3
M052X/6-31G(d,p)	+68.2	+3.8	+10.2
M06/6-31G	+38.6	-3.8	+3.2
M062X/6-311G	+41.8	-4.2	+3.5
M062X/6-311G(d,p)	+64.9	+0.7	+8.4
M062X/aug-cc-pVTZ	+74.9	+4.2	+11.2
M06HF/6-31G	-8.3	+10.9	+2.9
CIS/6-31G	+45.9	+7.9	+8.9
CIS/6-311G(d,p)	+67.0	+10.6	+12.8
CIS/aug-cc-pVTZ	+79.1	+14.2	+15.9

Table 9 Differences between calculated and experimental S_1 rotational constants (Δ = Calc − Exp, in MHz) for 2-Hydroxynaphthalene. Experimental values: $A' = 2769.1$, $B' = 821.8$, $C' = 634.0$ MHz.

Computational Method	$\Delta A'$ **(MHz)**	$\Delta B'$ **(MHz)**	$\Delta C'$ **(MHz)**
PBE1PBE/6-31G(d)	+38.8	-6.6	-2.2
PBEPBE/6-31G	-4.7	-18.7	-11.7
B97D3/6-31G	-6.1	-21.2	-13.3
B3LYP/6-311G	+33.5	-11.8	-5.6
BLYP/6-31G	-18.5	-25.0	-16.2
BP86/6-31G	-10.8	-21.2	-13.5
B3PW91/6-31G	+32.9	-9.3	-4.1
BMK/6-31G	-0.9	-12.7	-7.9
M05/6-31G	+37.9	-9.3	-3.9
M052X/6-31G	+27.7	-1.5	+0.3
M052X/6-31G(d,p)	+51.9	+2.5	+3.9
M06/6-31G	+48.5	-6.9	-1.9
M062X/6-311G	+20.8	-3.3	-1.2
M062X/6-311G(d,p)	+42.3	+2.0	+3.1
M062X/aug-cc-pVTZ	+69.6	+5.1	+6.3
M06HF/6-31G	+4.0	-0.7	-0.5
CIS/6-31G	+84.3	-2.9	+2.3
CIS/6-311G(d,p)	+90.8	+3.2	+6.3
CIS/aug-cc-pVTZ	+107.2	+6.9	+9.4

Table 10 Differences between calculated and experimental S_1 rotational constants (Δ = Calc − Exp, in MHz) for 1-Naphthoic acid. Experimental values: $A' = 1344.7$, $B' = 713.3$, $C' = 466.4$ MHz.

Computational Method	$\Delta A'$ **(MHz)**	$\Delta B'$ **(MHz)**	$\Delta C'$ **(MHz)**
PBE1PBE/6-31G(d)	-14.4	+10.9	+2.5
PBEPBE/6-31G	-41.7	+0.5	-7.2
B97D3/6-31G	-41.2	-4.3	-7.2
B3LYP/6-311G	-19.6	+5.3	-1.2
BLYP/6-31G	-48.6	-6.9	-9.2
BP86/6-31G	-45.1	-1.7	-6.6
B3PW91/6-31G	-19.2	+8.1	+0.8
BMK/6-31G	-24.6	+2.0	-2.5
M05/6-31G	-15.2	+7.6	+1.0
M052X/6-31G	-0.6	+10.9	+4.3
M052X/6-31G(d,p)	+4.7	+11.7	+5.2
M06/6-31G	-10.8	+10.7	+2.9
M062X/6-311G	-4.5	+9.5	+3.1
M062X/6-311G(d,p)	+2.0	+10.6	+4.4
M062X/aug-cc-pVTZ	+11.1	+13.6	+6.8
M06HF/6-31G	+15.6	-6.9	+10.3
CIS/6-31G	+17.5	+9.0	+5.6
CIS/6-311G(d,p)	+25.7	+10.5	+7.2
CIS/aug-cc-pVTZ	+30.3	+12.5	+8.7

Table 11 Differences between calculated and experimental S_1 rotational constants (Δ = Calc − Exp, in MHz) for 3-Toluidine. Experimental values: $A' = 3536.6$, $B' = 1788.8$, $C' = 1197.4$ MHz.

Computational Method	$\Delta A'$ **(MHz)**	$\Delta B'$ **(MHz)**	$\Delta C'$ **(MHz)**
PBE1PBE/6-31G(d)	+11.3	-4.0	-1.2
PBEPBE/6-31G	-35.9	-34.5	-19.5
B97D3/6-31G	-45.4	-38.1	-22.5
B3LYP/6-311G	-6.0	-12.6	-6.8
BLYP/6-31G	-61.8	-48.3	-28.7
BP86/6-31G	-48.3	-39.2	-23.1
B3PW91/6-31G	+0.7	-10.2	-5.2
BMK/6-31G	-38.1	-21.1	-14.4
M05/6-31G	-0.7	-9.3	-4.9
M052X/6-31G	+15.5	+2.1	+1.9
M052X/6-31G(d,p)	+39.7	+15.3	+11.5
M06/6-31G	+10.0	-2.1	+1.8
M062X/6-311G	+5.8	+1.9	+1.0
M062X/6-311G(d,p)	+26.8	+16.0	+7.3
M062X/aug-cc-pVTZ	+26.8	+21.7	+12.5
M06HF/6-31G	+7.1	+7.1	+4.3
CIS/6-31G	+40.2	+8.4	+7.5
CIS/6-311G(d,p)	+52.9	+18.7	+14.0
CIS/aug-cc-pVTZ	+150.6	+43.1	+35.7

Table 12 Differences between calculated and experimental S_1 rotational constants (Δ = Calc − Exp, in MHz) for 4-Methylanisole. Experimental values: $A' = 4682.0$, $B' = 984.5$, $C' = 818.5$ MHz.

Computational Method	$\Delta A'$ **(MHz)**	$\Delta B'$ **(MHz)**	$\Delta C'$ **(MHz)**
PBE1PBE/6-31G(d)	-108.0	-7.9	-5.3
PBEPBE/6-31G	-233.0	-27.0	-7.5
B97D3/6-31G	-170.1	-31.3	-23.6
B3LYP/6-311G	-109.8	-18.8	-13.1
BLYP/6-31G	-243.0	-40.6	-18.8
BP86/6-31G	-242.6	-30.4	-10.9
B3PW91/6-31G	-115.1	-13.1	-9.3
BMK/6-31G	-160.7	-16.1	-12.6
M05/6-31G	-100.9	-13.8	-9.4
M052X/6-31G	-113.2	-3.9	-2.7
M052X/6-31G(d,p)	-100.0	+12.9	+9.5
M06/6-31G	-111.4	-4.4	-3.2
M062X/6-311G	-106.1	-6.1	-3.9
M062X/6-311G(d,p)	-100.7	+10.7	+8.0
M062X/aug-cc-pVTZ	-99.4	+5.7	+7.8
M06HF/6-31G	-279.6	-16.4	+24.1
CIS/6-31G	-153.2	-22.0	+19.7
CIS/6-311G(d,p)	-149.6	+0.2	+37.1
CIS/aug-cc-pVTZ	-113.1	+1.8	+37.9

Table 13 Differences between calculated and experimental S_1 rotational constants (Δ = Calc − Exp, in MHz) for 9-Fluorenemethanol. Experimental values: $A' = 920.6$, $B' = 556.0$, $C' = 366.9$ MHz.

Computational Method	$\Delta A'$ **(MHz)**	$\Delta B'$ **(MHz)**	$\Delta C'$ **(MHz)**
PBE1PBE/6-31G(d)	-20.3	+0.0	-11.1
PBEPBE/6-31G	-40.8	-4.4	-19.1
B97D3/6-31G	-47.3	-4.9	-19.5
B3LYP/6-311G	-29.5	-1.4	-14.2
BLYP/6-31G	-50.4	-7.8	-21.7
BP86/6-31G	-41.0	-6.0	-19.6
B3PW91/6-31G	-22.2	-1.9	-11.8
BMK/6-31G	-24.9	-4.8	-14.8
M05/6-31G	-25.8	+0.0	-12.5
M052X/6-31G	-10.1	-1.4	-7.3
M052X/6-31G(d,p)	-1.2	-0.6	-2.7
M06/6-31G	-16.0	-0.6	-8.2
M062X/6-311G	-3.7	-4.4	-5.3
M062X/6-311G(d,p)	+0.0	-2.1	-3.1
M062X/aug-cc-pVTZ	+2.7	+1.3	+1.6
M06HF/6-31G	+0.0	-6.3	-2.0
CIS/6-31G	-22.8	+5.8	-9.7
CIS/6-311G(d,p)	-21.3	+9.1	-7.7
CIS/aug-cc-pVTZ	-21.3	+12.3	-5.6

References

1. D. W. Pratt, "High resolution spectroscopy in the gas phase: even large molecules have well-defined shapes," *Annual review of physical chemistry*, vol. 49, no. 1, pp. 481–530, 1998.
2. W. L. Meerts and M. Schmitt, "Application of genetic algorithms in high-resolution laser spectroscopy," *International Reviews in Physical Chemistry*, vol. 25, no. 3, pp. 353–406, 2006.
3. W. Leo Meerts and M. Schmitt, "Application of genetic algorithms in automated assignments of high-resolution spectra," *International Reviews in Physical Chemistry*, vol. 25, no. 3, pp. 353–406, 2006.
4. M. J. Frisch, G. W. Trucks, H. B. Schlegel, G. E. Scuseria, M. A. Robb, J. R. Cheeseman, G. Scalmani, V. Barone, G. A. Petersson, H. Nakatsuji, X. Li, M. Caricato, A. V. Marenich, J. Bloino, B. G. Janesko, R. Gomperts, B. Mennucci, H. P. Hratchian, J. V. Ortiz, A. F. Izmaylov, J. L. Sonnenberg, D. Williams-Young, F. Ding, F. Lipparini, F. Egidi, J. Goings, B. Peng, A. Petrone, T. Henderson, D. Ranasinghe, V. G. Zakrzewski, J. Gao, N. Rega, G. Zheng, W. Liang, M. Hada, M. Ehara, K. Toyota,

R. Fukuda, J. Hasegawa, M. Ishida, T. Nakajima, Y. Honda, O. Kitao, H. Nakai, T. Vreven, K. Throssell, J. A. Montgomery, Jr., J. E. Peralta, F. Ogliaro, M. J. Bearpark, J. J. Heyd, E. N. Brothers, K. N. Kudin, V. N. Staroverov, T. A. Keith, R. Kobayashi, J. Normand, K. Raghavachari, A. P. Rendell, J. C. Burant, S. S. Iyengar, J. Tomasi, M. Cuzzocrea, R. Cammi, C. Pomelli, C. Adamo, S. Clifford, J. Ochterski, G. A. Petersson, P. Ayala, Q. Cui, K. Morokuma, P. Salvador, J. J. Dannenberg, D. K. Malick, A. D. Daniels, O. Farkas, J. B. Foresman, J. V. Ortiz, J. Cioslowski, and D. J. Fox, "Gaussian 16, revision c.01." Gaussian, Inc., Wallingford CT, 2016.

5. E. Runge and E. K. Gross, "Density-functional theory for time-dependent systems," *Physical review letters*, vol. 52, no. 12, p. 997, 1984.
6. M. E. Casida, "Time-dependent density functional response theory for molecules," in *Recent Advances In Density Functional Methods: (Part I)*, pp. 155–192, World Scientific, 1995.
7. J. B. Foresman, M. Head-Gordon, J. A. Pople, and M. J. Frisch, "Toward a systematic molecular orbital theory for excited states," *The Journal of Physical Chemistry*, vol. 96, no. 1, pp. 135–149, 1992.
8. J. Johnson, K. Jordan, D. Plusquellic, and D. Pratt, "High resolution s 1← s fluoescence excitation spectra of the 1-and 2-hydroxynaphthalenes. distinguishing the cis and trans rotamers," *The Journal of chemical physics*, vol. 93, no. 4, pp. 2258–2273, 1990.
9. S. Jagannathan and D. W. Pratt, "The fluorescence excitation spectrum of 1-naphthoic acid at rotational resolution: S and s 1 potential energy surfaces along the r–cooh torsional coordinate," *The Journal of chemical physics*, vol. 100, no. 3, pp. 1874–1883, 1994.
10. C. Kang, J. T. Yi, and D. W. Pratt, "High resolution electronic spectra of 7-azaindole and its ar atom van der waals complex," *The Journal of chemical physics*, vol. 123, no. 9, 2005.
11. L. Alvarez-Valtierra, J. T. Yi, and D. W. Pratt, "Rotationally resolved electronic spectra of 2-and 3-methylanisole in the gas phase: a study of methyl group internal rotation," *The Journal of Physical Chemistry B*, vol. 110, no. 40, pp. 19914–19922, 2006.
12. P. J. Morgan, L. Alvarez-Valtierra, and D. W. Pratt, "High resolution electronic spectroscopy of o-and m-toluidine in the gas phase. barrier height determinations for the methyl group torsional motions," *The Journal of Physical Chemistry A*, vol. 113, no. 47, pp. 13221–13226, 2009.
13. L. Alvarez-Valtierra, J. T. Yi, and D. W. Pratt, "Lifetime broadening in the rotationally resolved electronic spectra of dibenzothiophene, 2, 5-diphenylfuran, and 2, 5-diphenyl-1, 3, 4-oxadiazole in the gas phase. intersystem crossing dynamics in the statistical limit.," *The Journal of Physical Chemistry A*, vol. 113, no. 11, pp. 2261–2267, 2009.
14. P. J. Morgan, L. Alvarez-Valtierra, and D. W. Pratt, "High resolution electronic spectroscopy of 4-methylanisole in the gas phase. barrier height determinations for the methyl group torsional motion," *Physical Chemistry Chemical Physics*, vol. 12, no. 29, pp. 8323–8328, 2010.
15. J. A. Thomas, L. Alvarez-Valtierra, and D. W. Pratt, "Re-examination of the rotationally resolved spectra of the electronic origin and several vibronic bands of 1, 3-benzodioxole," *Chemical Physics Letters*, vol. 490, no. 4-6, pp. 109–115, 2010.
16. D. M. Miller, J. W. Young, P. J. Morgan, and D. W. Pratt, "High resolution electronic spectroscopy of 9-fluorenemethanol in the gas phase: New insights into the properties of π-hydrogen bonds," *The Journal of chemical physics*, vol. 133, no. 12, 2010.
17. J. P. Perdew, K. Burke, and M. Ernzerhof, "Generalized gradient approximation made simple," *Physical review letters*, vol. 77, no. 18, p. 3865, 1996.
18. A. D. Becke, "Density-functional exchange-energy approximation with correct asymptotic behavior," *Physical review A*, vol. 38, no. 6, p. 3098, 1988.
19. S. Grimme, J. Antony, S. Ehrlich, and H. Krieg, "A consistent and accurate ab initio parametrization of density functional dispersion correction (dft-d3) for the 94 elements h-pu," *The Journal of Chemical Physics*, vol. 132, no. 15, p. 154104, 2010.
20. Y. Zhao, N. E. Schultz, and D. G. Truhlar, "Design of density functionals by combining nonlocal exchange with local density approximation and generalized gradient approximation correlation," *Journal of Chemical Theory and Computation*, vol. 2, no. 2, pp. 364–382, 2006.

21. Y. Zhao and D. G. Truhlar, "The m06 suite of density functionals for main group thermochemistry, thermochemical kinetics, noncovalent interactions, excited states, and transition elements," *Theoretical Chemistry Accounts*, vol. 120, no. 1, pp. 215–241, 2008.
22. A. D. Becke, "Density-functional thermochemistry. iii. the role of exact exchange," *The Journal of Chemical Physics*, vol. 98, no. 7, pp. 5648–5652, 1993.
23. C. Adamo and V. Barone, "Toward reliable density functional methods without adjustable parameters: The pbe0 model," *The Journal of Chemical Physics*, vol. 110, no. 13, pp. 6158–6170, 1999.
24. A. D. Becke, "A new mixing of hartree–fock and local density-functional theories," *The Journal of Chemical Physics*, vol. 93, no. 2, pp. 1372–1377, 1993.
25. A. D. Boese and J. M. L. Martin, "Development of density functionals for thermochemical kinetics," *The Journal of Chemical Physics*, vol. 121, no. 8, pp. 3405–3416, 2004.
26. W. J. Hehre, R. Ditchfield, and J. A. Pople, "Self-consistent molecular orbital methods. xii. further extensions of gaussian-type basis sets for use in molecular orbital studies of organic molecules," *The Journal of Chemical Physics*, vol. 56, no. 5, pp. 2257–2261, 1972.
27. P. C. Hariharan and J. A. Pople, "The influence of polarization functions on molecular orbital hydrogenation energies," *Theoretica Chimica Acta*, vol. 28, no. 3, pp. 213–222, 1973.
28. R. Krishnan, J. S. Binkley, R. Seeger, and J. A. Pople, "Self-consistent molecular orbital methods. xx. a basis set for correlated wave functions," *The Journal of Chemical Physics*, vol. 72, no. 1, pp. 650–654, 1980.
29. T. Clark, J. Chandrasekhar, G. W. Spitznagel, and P. V. R. Schleyer, "Efficient diffuse function-augmented basis sets for anions and weakly bound complexes. on-hydrogen atoms," *Journal of Computational Chemistry*, vol. 4, no. 3, pp. 294–301, 1983.
30. T. H. Dunning, "Gaussian basis sets for use in correlated molecular wave functions. i. the atoms boron through neon and hydrogen," *The Journal of Chemical Physics*, vol. 90, no. 2, pp. 1007–1023, 1989.
31. R. A. Kendall, T. H. Dunning, and R. J. Harrison, "Electron affinities of the first-row atoms revisited, as represented by systematic basis sets and relativistic corrections," *The Journal of Chemical Physics*, vol. 96, no. 9, pp. 6796–6806, 1992.
32. K. L. Lee and M. McCarthy, "Bayesian analysis of theoretical rotational constants from low-cost electronic structure methods," *The Journal of Physical Chemistry A*, vol. 124, no. 5, 2020.
33. A. B. Myers and T. R. Rizzo, "Laser techniques in chemistry," *(No Title)*, 1995.
34. D. F. Plusquellic, "User guide to the jb95 spectral fitting program," 2002.